COORDINATED CONTROL OF THE TWO-PHASE VIBRATION MODE OF TWUSM BASED ON DISCRETE CONTACT MODEL

KAI JING, JIN GUO, ZHAOMING LEI AND JING LIANG

Department of New Energy Science and Engineering
Hebei University of Technology
No. 8, Guangrong Road, Hongqiao District, Tianjin 300130, P. R. China
jingkai_1082@126.com

ABSTRACT. *A coordinated control method of travelling-wave ultrasonic motor for improving the servo control performance has been put forward. According to the analysis of the dynamics of the motor by the proposed discrete contact model, which focuses on the discontinuous tooth-shaped structure on the stator surface to solve the contact effects, the two-phase vibration mode directly affects the performance of the motor. Then a coordinated control method of the two-phase vibration mode by adjusting one phase vibration mode with another phase as a reference is achieved by a proportional-resonant (PR) controller. At last, the control performances of reducing the torque ripple and improving the control accuracy are verified by the simulations and experiments.*
Keywords: Travelling-wave ultrasonic motor, Coordinated control, Vibration mode, Discrete contact model

1. **Introduction.** Travelling-wave ultrasonic motor (written briefly TWUSM) is a kind of representative ultrasonic motor, which has the advantages of high torque density, high position resolution, fast dynamic response and no electromagnetic interference. As a new driving device, it has begun to replace the conventional miniature electromagnetic motor in the field of high precision transmission control, such as medicine and aerospace. It is especially suitable for direct drive of precision system, such as camera lens focus, high-precision tympanic membrane intubation device and lunar rover spectrometer drive device.

However, being different from electromagnetic motor, the operating mechanism of TWU-SM depends on the inverse piezoelectric effect of piezoelectric material, with which a traveling wave is excited by two-phase high frequency voltages in the stator and the friction force is generated in the contact interface between stator and rotor that the rotor is driven. Nonlinearity and multidisciplinary cross of the motor increase the difficulty for research.

The complex TWUSM model makes it difficult to control directly. Some researchers directly used the qualitative analysis and experimental test to control the motor by the relationship of the amplitude, frequency and phase of the input voltages and the output torque, speed and position [1-3]. Some other researchers proposed the control methods by the identification model based on the input and output date. Mo et al. [4] proposed a model reference adaptive control based on a three order linear model of the input voltages and the output position. Liang et al. [5,6] put forward a "voltage-position" model which is divided into linear and nonlinear parts, and an LQR assisted PID control is developed to control the position. Shi et al. [7-9] have studied a nonlinear Hammerstein model of TWUSM and implemented control by the robust control strategy. However, the control methods above only focus on the input and output characteristics of the motor, which

ignore the piezoelectric effect, the stator vibration and the contact dynamics in TWUSMs, so the control performance is difficult to improve.

In this paper, a novel vibration modes coordinated control method of TWUSMs has been proposed by analyzing the operation dynamics and modeling the motor with contact discretization. By the method, the dynamic torque performance and the control accuracy are improved that the method is more suitable for precision system in application. The paper is organized as follows. In Section 2, an exhaustive study about the discrete contact model of TWUSM is contributed. Section 3 analyzes the effect of the two-phase vibration mode by the model and presents the coordinated control of the two-phase vibration mode based on PR controller. The simulations and experiments are carried out in Section 4, which is to verify the control performance of the new method. Section 5 summarizes the whole paper.

2. **Discrete Contact Model for TWUSM.** By analyzing the operating mechanism of TWUSM, the key to modeling TWUSM is to deal with the contact action between the stator and rotor. The strong nonlinearity and coupling of the contact make it difficult and complex to describe with analytical method. To obtain an accurate description of TWUSMs, this paper focuses on the discontinuous tooth-shaped structure on the stator, and a discrete contact modeling method has been put forward to simplify the complex calculation.

The "elasticity-damping system" is usually used to describe the stator of TWUSMs, which satisfies the following electromechanical coupling equation and current equations

$$\boldsymbol{M}_{\mathrm{s}}\ddot{\boldsymbol{w}} + \boldsymbol{D}_{\mathrm{s}}\dot{\boldsymbol{w}} + \boldsymbol{C}_{\mathrm{s}}\boldsymbol{w} = \Theta\boldsymbol{u} + \boldsymbol{F}_{\mathrm{C}} \tag{1}$$

$$\boldsymbol{i} = \boldsymbol{R}_{\mathrm{d}}^{-1}\boldsymbol{u} + \boldsymbol{C}_{\mathrm{d}}\dot{\boldsymbol{u}} + \Theta\dot{\boldsymbol{w}} \tag{2}$$

where $\boldsymbol{u} = [u_{\mathrm{A}}, u_{\mathrm{B}}]^{\mathrm{T}}$ is the two-phase excitation voltage; $\boldsymbol{i} = [i_{\mathrm{A}}, i_{\mathrm{B}}]^{\mathrm{T}}$ is the exciting current; and $\boldsymbol{F}_{\mathrm{C}} = [f_{\mathrm{CA}}, f_{\mathrm{CB}}]^{\mathrm{T}}$ means the contact modal force in the interface of two phases. The matrixes $\boldsymbol{M}_{\mathrm{s}}$, $\boldsymbol{D}_{\mathrm{s}}$ and $\boldsymbol{C}_{\mathrm{s}}$ respectively stand for the two-phase modal mass, modal damping and modal stiffness, which are all diagonal matrixes; $\boldsymbol{D}_{\mathrm{s}}$ and $\boldsymbol{C}_{\mathrm{s}}$ are modal damping matrix and modal stiffness matrix and Θ is electromechanical coupling coefficient. In addition, the parameters in (1) and (2) can be measured and calculated by the admittance circle method.

The two-phase vibration mode $\boldsymbol{w}$ excited by supply voltages will generate a traveling wave in the stator elastomer, which cause the movements of the points in the stator surface. The movements can be described in the r-θ-z cylindrical coordinate system

$$\boldsymbol{u} = \begin{bmatrix} u_{\mathrm{sr}} \\ u_{\mathrm{s\theta}} \\ u_{\mathrm{sz}} \end{bmatrix} = \boldsymbol{\Phi} \cdot \boldsymbol{w} = \begin{bmatrix} \phi_{\mathrm{r}}(r,z)\cos\left(k\hat{\theta}\right) & \phi_{\mathrm{r}}(r,z)\sin\left(k\hat{\theta}\right) \\ -\phi_{\mathrm{\theta}}(r,z)\sin\left(k\hat{\theta}\right) & \phi_{\mathrm{\theta}}(r,z)\cos\left(k\hat{\theta}\right) \\ \phi_{\mathrm{z}}(r,z)\cos\left(k\hat{\theta}\right) & \phi_{\mathrm{z}}(r,z)\sin\left(k\hat{\theta}\right) \end{bmatrix} \begin{bmatrix} w_{\mathrm{A}} \\ w_{\mathrm{B}} \end{bmatrix} \tag{3}$$

where $\boldsymbol{\Phi}$ is the modal matrix if the two phases; k is the wave number.

The rotor is driven by the contact force and moves in the circumferential and axial direction which follows the following equations respectively:

$$M_{\mathrm{R}}\ddot{z}_{\mathrm{R}} + D_{\mathrm{R}}\dot{z}_{\mathrm{R}} = F_{\mathrm{z}} - F_{\mathrm{pre}} \tag{4}$$

$$J_{\mathrm{R}}\frac{d\omega_{\mathrm{R}}}{dt} = T_{\mathrm{e}} - T_{\mathrm{load}} \tag{5}$$

where M_{R}, D_{R} and J_{R} mean the mass, axial damping and rotational inertia of rotor respectively. z_{R} and ω_{R} are the axial displacement and angular velocity respectively. F_{z} is axial contact force, T_{e} is the output torque, F_{pre} is the pre-pressure, and T_{load} is the load torque.

In order to solve the contact between stator and rotor, a discrete contact modeling method is proposed by making the surface contact of each tooth equivalent to discrete point contact. Considering the symmetry of the traveling wave superimposed by the two-phase modes w_A and w_B, the contact relationship can be analyzed in a wavelength. The l discrete points under a wavelength corresponding to the stator teeth are used to solve the dynamics. The axial displacement of the discrete points can be expressed as follows

$$u_{sz}^{(j)} = \Phi_z \left(w_A \cos k\hat{\theta}^{(j)} + w_B \sin k\hat{\theta}^{(j)} \right) = \Phi_z w(t) \cos \left(k\hat{\theta}^{(j)} - k\theta_c \right) \tag{6}$$

where $W = \sqrt{w_A^2 + w_B^2}$, $\theta_c = \dfrac{1}{k}\text{atan}\left(\dfrac{w_B}{w_A}\right)$ and $j = 1, 2, \ldots, l-1$. The expression can be simplified by coordinates transform.

$$u_{sz}^{(j)} = \Phi_z w(t) \cos \left(k\theta^{(j)} \right) \tag{7}$$

From the contact state in Figure 1, the axial displacement of the non-deformed surface of the friction layer z_1 that is also called dynamic displacement can be expressed by $k\theta_0$.

$$z_1 = \Phi_z w(t) \cos(k\theta_0) \tag{8}$$
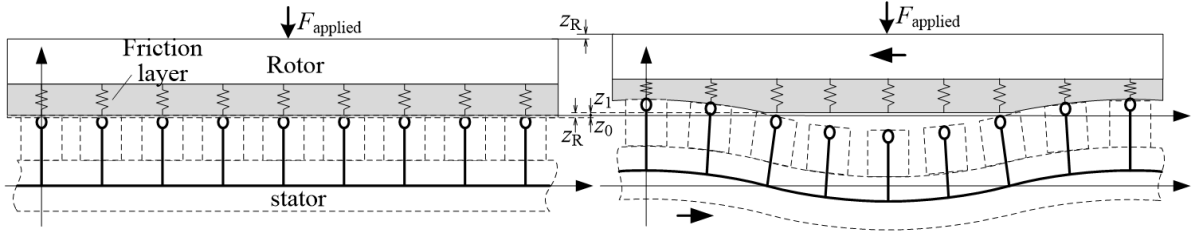
FIGURE 1. Contact state of the stator and rotor in TWUSM

The interaction between the stator and rotor only exists in the contact region $[-k\theta_0, k\theta_0]$. The axial discrete pressure of each point can be expressed with the same equation, but the equivalent stiffness $c_N^{(j)}$ is different for different contact states.

$$f_n^{(j)} = c_N^{(j)} u_{sz}^{(j)} - c_N^{(j)} z_1 \triangleq f_1^{(j)} - c_N^{(j)} z_1 \tag{9}$$

Hence, the axial pressure F_z can be gained:

$$F_z = k \sum_{j=0}^{l-1} f_n^{(j)} = k \sum_{j=0}^{l-1} f_1^{(j)} - z_1 \cdot k \sum_{j=0}^{l-1} c_N^{(j)} \triangleq F_1 - C_R z_1 \tag{10}$$

Therefore, z_1 and the contact boundary $k\theta_0$ will be gotten from Formulas (4) and (8).

The frictions in tangential direction for each discrete contact point are proportional to the axial pressures:

$$f_\tau^{(j)} = \mu f_n^{(j)} \tag{11}$$

where μ is dynamic friction coefficient of friction between stator and rotor. The direction of the friction is determined by radial and circumferential velocity of the discrete point.

$$\begin{cases} f_{\tau r}^{(j)} = \dfrac{v_{sr}}{\sqrt{(v_{s\theta} - v_R)^2 + v_{sr}^2}} f_\tau^{(j)} \\ f_{\tau\theta}^{(j)} = \dfrac{v_{s\theta} - v_R}{\sqrt{(v_{s\theta} - v_R)^2 + v_{sr}^2}} f_\tau^{(j)} \end{cases} \tag{12}$$

The output torque is obtained by circumferential friction:

$$T_e = r_c k \sum_{j=0}^{l-1} f_{\tau\theta}^{(j)} \tag{13}$$

In addition, the interface contact modal force $\boldsymbol{F}_{\mathrm{C}}$ is expressed by virtual work principle

$$\boldsymbol{F}_{\mathrm{C}} = k \sum_{j=0}^{l-1} \boldsymbol{\Phi}^{(j)T} \cdot \boldsymbol{f}^{(j)} \tag{14}$$

Thus, the hybrid model of TWUSM is shown in Figure 2.

A TRUM-60A types motor will be used for the study and analysis of the characteristics of the discrete contact model. Some parameters of the motor are listed in Table 1.

By comparing simulation curves with mechanical characteristics and efficiency data obtained by experimental measurements, in the three figures in Figure 3, the measuring data points which are marked with "+" are around the simulation curve, which prove that the modeling method can truly reflect the mechanism of the motor.

FIGURE 2. Discrete contact model of TWUSM

TABLE 1. Parameters of TWUSM modeling

Symbol	Parameters	Value
Θ	Electromechanical coupling coefficient	0.242
k	Travelling-wave number	9
m	Stator teeth number	72
μ	Coefficient of friction between stator and rotor	0.2
$R_{\mathrm{dA}}/R_{\mathrm{dB}}$	Dielectric loss resistance of phase A/B	8.777/39.53kΩ
$C_{\mathrm{dA}}/C_{\mathrm{dB}}$	Static capacitance of phase A/B	8.748/7.400nF
M_{R}	Rotor mass	0.0335kg
D_{R}	Axial damping of rotor	1500Ns/m
r_{c}	Average contact radius	27.58mm
J	Rotor inertia	14×10^{-6}kg·m^2

FIGURE 3. Mechanical characteristics of experiment and simulation

3. **Two-Phase Vibration Mode Coordination Control of TWUSM for the Servo Control.** TWUSM is usually used for low-speed high-torque precision direct drive control, in which the control performances are determined by the torque. Generally, the two-phase supply voltages are with the same constant amplitude and fixed phases and the frequency is regulated to control the speed as well as the position of the motor. However, the actual parameters of the two phases are not completely symmetrical, the method mentioned above will lead to the large torque ripple, which will affect the precision of the control performance.

The output torque of the motor is analyzed by the model built with above parameters that the two-phase parameters are greatly different from each other. When the supply voltages are with the same amplitude and $\pi/2$ phase difference, the excited two-phase vibration mode is shown as the top figure in Figure 4(a) of which the amplitudes are not equal and the output torque is shown as the dotted line in Figure 4(b) with the large torque ripple. When the voltages are adjusted so that the amplitudes of the two-phase vibration mode become the same and the phase difference is $\pi/2$, which is shown in the bottom figure in Figure 4(a), the torque ripple becomes smaller in Figure 4(b).

(a) Waveform of vibration mode   (b) Waveform of the torque
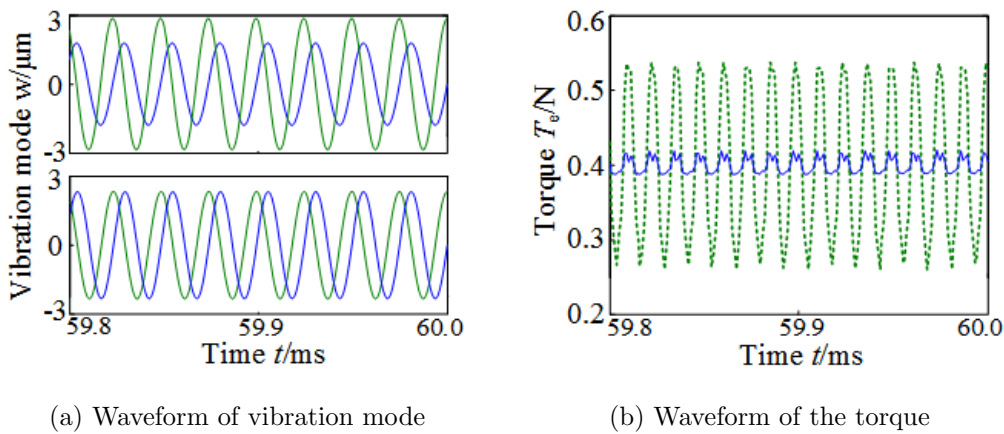
FIGURE 4. Relationship of two-phase vibration mode and the torque ripple

In summary, it is the key to improving the operating performance to control the vibration mode to meet the idea condition of equal amplitude and $\pi/2$ phase difference. So, a coordination control method for the two-phase vibration mode is proposed.

Firstly, because the two-phase vibration mode cannot be directly measured, an observer is deduced by Formula (2), so that the two-phase vibration mode will be got by measuring the voltages and the currents. The observer is expressed as follows:

$$\begin{cases} w_{\mathrm{A}} = \dfrac{1}{\Theta} \int \left(i_{\mathrm{A}} - \dfrac{u_{\mathrm{A}}}{R_{\mathrm{dA}}} - C_{\mathrm{dA}} \dfrac{du_{\mathrm{A}}}{dt} \right) dt \\ w_{\mathrm{B}} = \dfrac{1}{\Theta} \int \left(i_{\mathrm{B}} - \dfrac{u_{\mathrm{B}}}{R_{\mathrm{dB}}} - C_{\mathrm{dB}} \dfrac{du_{\mathrm{B}}}{dt} \right) dt \end{cases} \tag{15}$$

The parameters R_{dA}, R_{dB}, C_{dA}, C_{dB} in the expression are almost independent of environment change, which ensure the high accuracy of the observation results.

A coordinate control method for the two-phase vibration mode is proposed to achieve the expected state. The mode response can be analyzed by the model simulation and the one phase that the mode amplitude is less than the other when powered with the same voltage is selected as the reference to avoid the voltage exceeding the maximum. Assume that phase A is the reference, then phase B is the controlled one. When the vibration modes of phase A are observed it will be shifted by $\pm\pi/2$ as the given.

Determined by the running direction. The observed value of phase B is as the feedback to be controlled to track the given. The control structure is shown in Figure 5, in which
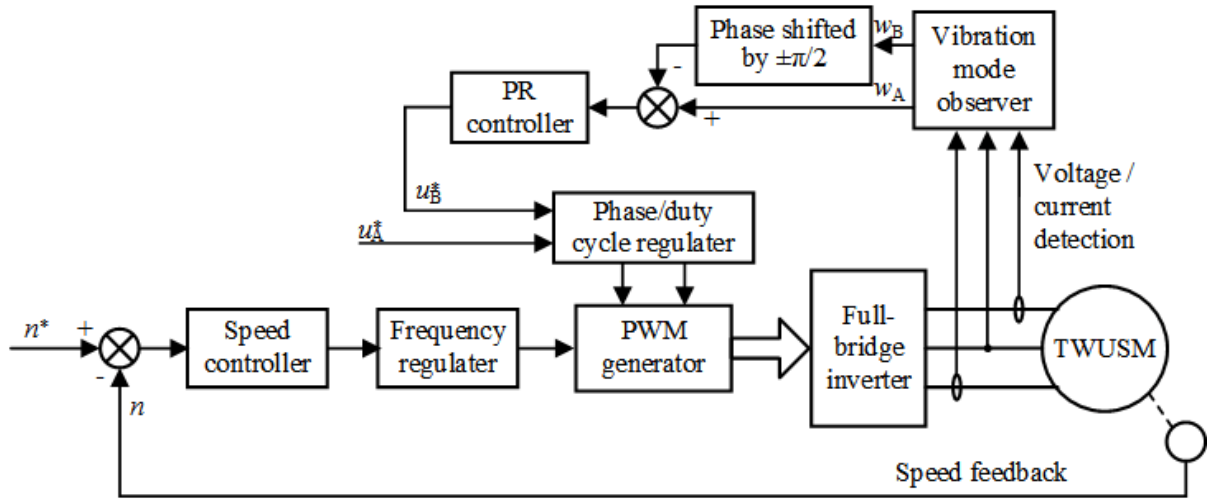
FIGURE 5. Block for two-phase vibration mode coordination control

the speed is controlled by frequency and the full-bridge inverter is adopted as the driven circuit.

For controlling the B-phase vibration mode changed with the given sinusoidal law, the traditional proportional-integral (PI) control cannot achieve the zero error tracking, but the proportional-resonant (PR) control can realize the performance for a particular frequency, which is used for directly tracking control of AC voltage and current [10-12]. The transfer function of the PR controller is expressed as the following:

$$G_{\mathrm{PR}}(s) = k_{\mathrm{p}} + \frac{k_{\mathrm{i}}s}{s^2 + \omega_0^2} \tag{16}$$

where k_{p}, k_{i} are equivalent to the proportional and integral coefficient in PI control respectively, and ω_0 is the resonant frequency that if $\omega_0 = 0$, it becomes a PI control.

However, the infinite gain at the resonant frequency leads to the PR controller unavailable in reality, so a quasi-PR controller is adopted to avoid the defect and get large gain in the interval near the resonant frequency. The expression of quasi-PR controller is

$$G_{\mathrm{qPR}}(s) = k_{\mathrm{p}} + \frac{k_{\mathrm{i}}s}{s^2 + 2\omega_{\mathrm{c}}s + \omega_0^2} \tag{17}$$

where ω_{c} is the low pass filter frequency, which can be set to achieve a large bandwidth for the working frequency of TWUSMs. So the two-phase vibration mode can be coordinately controlled achieving the zero error tracking to meet the expected requirements.

4. **Simulations and Experiments.** The simulation model for control is built based on the parameters of the motor typed TRUM-60A in Table 1. The output voltage of the full-bridge inverter is 110V, and the speed controller is adopted of PI regulator. The equal voltage amplitude control method and the vibration mode coordinated control method proposed in the paper will be comparatively analyzed by simulations and experiments.

Simulation results in steady state are shown in Figure 6 and Figure 7, where the phase voltage, current, vibration mode and output torque waveform are studied comparatively.

By regulating the duty ratio of the full-bridge driven circuit, the driven voltages with the same amplitude and $\pi/2$ phase difference are shown in Figure 6(a). However, due to the inconsistency of the stator structure parameters, the currents and the vibration modes of phases A and B are not the same. It is worth noting that the amplitude of the current of phase A is greater than it of phase B in Figure 6(b), but the vibration mode waveform shows that the amplitude of phase A is less than B. And the unequal vibration mode amplitudes lead to the large torque ripple in Figure 6(d), while the phenomenon
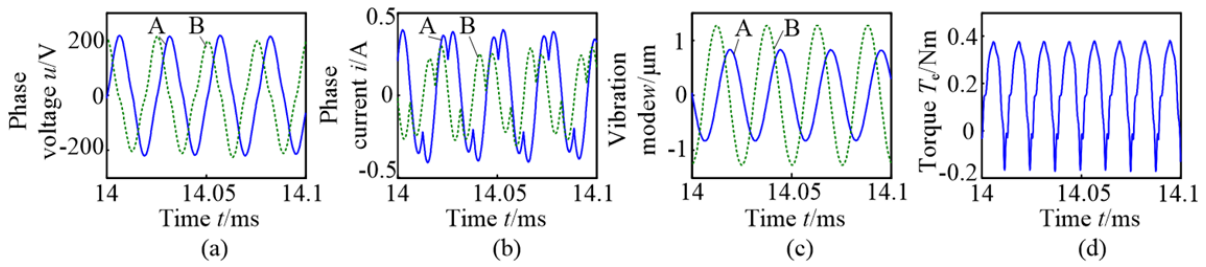
FIGURE 6. Control result by the traditional method
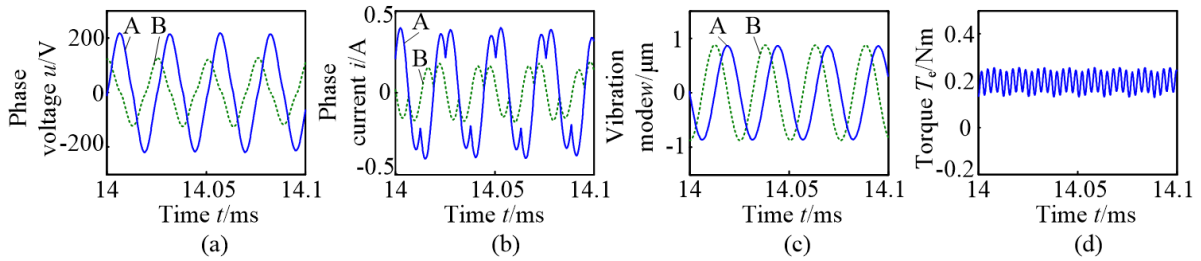
FIGURE 7. Control result by the vibration mode coordinated control

(a) Experimental platform   (b) Voltage of the inverter   (c) Phase voltages   (d) Phase currents
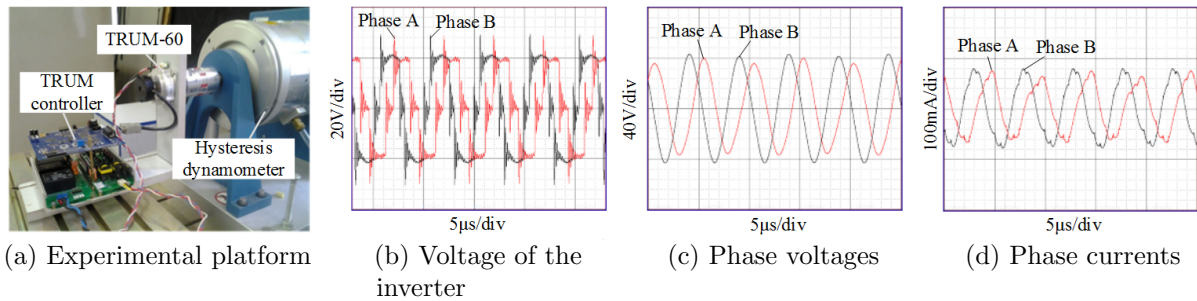
FIGURE 8. Experimental platform and electric curve of the coordinated control

(a) Speed curve   (b) Speed curve   (c) Torque curve   (d) Torque curve
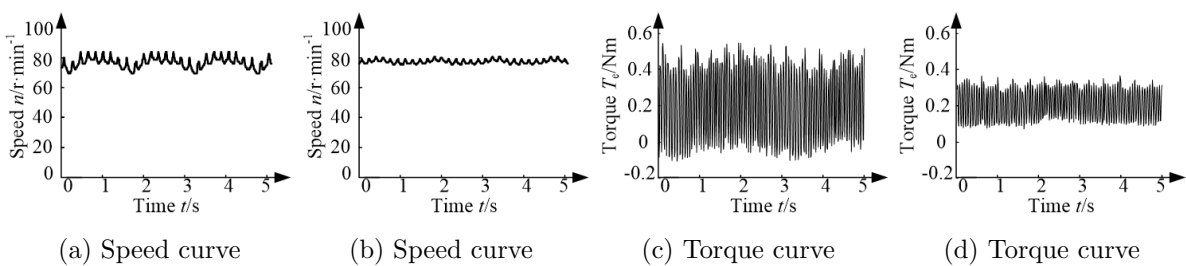
FIGURE 9. Comparison of experiments curves

is improved by the coordinated method proposed in the paper, in which the voltage of phase B is regulated by controlling the vibration modes with the same amplitude and $\pi/2$ phase difference shown in Figure 7.

The experiments have been done on the platform of TWUSM shown in Figure 8(a). By the waveform recorder, the measured waves of the output voltages of the inverter, two-phase voltages and the currents are shown in Figures 8(b), 8(c) and 8(d), that the amplitude of phase B is regulated to improve the vibration model.

The conditions of the experiment are the same to one of the simulations. When load torque is 0.2Nm and driving amplitude is constant, the output torque curve under usually control and the method proposed in this paper can be got, as shown in Figure 9.

It can be seen clearly from the picture, the speed ripple and the output torque ripple by the proposed method in Figures 9(b) and 9(d) are smaller than the control method in common Figures 9(a) and 9(c), and the motor runs more smoothly.

5. **Conclusions.** In this paper, a discrete contact model is established to analyze the dynamics of TWUSMs. Then a new control method for travelling-wave ultrasonic motors by coordinately controlling of the two-phase vibration mode has been put forward to improve the servo control performance. In this method, one phase vibration mode is used as a reference to dynamically adjust the amplitude and phase of the other phases by controlling the voltage by PR control. The method can control the stator vibration of TWUSMs directly and improve the torque ripple. The simulations and experiments verified the effectiveness of vibration mode coordinated control method.

REFERENCES

[1] G. Kang, Q. Zhou, K. Fan et al., Rotary inertial navigation system turntable based on ultrasonic motor, *Journal of Chinese Inertial Technology*, vol.24, no.4, pp.421-426, 2016.

[2] S. Pan, L. Jian and W. Huang, The control method of ultrasonic motor direct driving motorized revolving nosepiece, *Journal of Vibration, Measurement & Diagnosis*, vol.36, no.4, pp.796-800, 2016.

[3] T. Kai, K. Sakuma, Y. Nakamura et al., High-speed positioning methods of an ultrasonic motor by input shaping filter and Bang-Bang control, *SICE Conference*, pp.1093-1098, 2011.

[4] J. S. Mo, Z. C. Qiu, J. Y. Wei et al., Adaptive positioning control of an ultrasonic linear motor system, *Robotics & Computer Integrated Manufacturing*, vol.44, pp.156-173, 2017.

[5] K. K. Tan, W. Liang, S. Huang et al., Precision control of piezoelectric ultrasonic motor for myringotomy with tube insertion, *Journal of Dynamic Systems Measurement & Control*, vol.137, no.6, pp.164-169, 2015.

[6] W. Liang, S. Huang, S. Chen et al., Precision motion control of a linear piezoelectric ultrasonic motor stage, *IEEE/ASME International Conference on Advanced Intelligent Mechatronics*, pp.164-169, 2013.

[7] J. Shi and F. Lv, Self-tuning nonlinear generalized predictive speed control of ultrasonic motors, *Proc. of the CSEE*, vol.32, no.27, pp.66-72, 2012.

[8] J. Shi, J. Zhao, J. Huang et al., Identification of ultrasonic motor's nonlinear Hammerstein model, *Journal of Control, Automation and Electrical Systems*, vol.25, no.5, pp.537-546, 2014.

[9] J. Shi and D. You, Characteristic model of travelling wave ultrasonic motor, *Ultrasonics*, vol.54, no.2, pp.725-730, 2014.

[10] P. Alemi, C. J. Bae and D. C. Lee, Resonance suppression based on PR control for single-phase grid-connected inverters with LLCL filters, *IEEE Journal of Emerging & Selected Topics in Power Electronics*, vol.4, no.2, pp.459-467, 2016.

[11] H. Komurcugil, N. Altin, S. Ozdemir et al., Lyapunov-function and proportional-resonant-based control strategy for single-phase grid-connected VSI with LCL filter, *IEEE Trans. Industrial Electronics*, vol.63, no.5, pp.2838-2849, 2015.

[12] T. Ye, N. Y. Dai, C. S. Lam et al., Analysis, design, and implementation of a quasi-proportional-resonant controller for a multifunctional capacitive-coupling grid-connected inverter, *IEEE Trans. Industry Applications*, vol.52, no.5, pp.4269-4280, 2016.